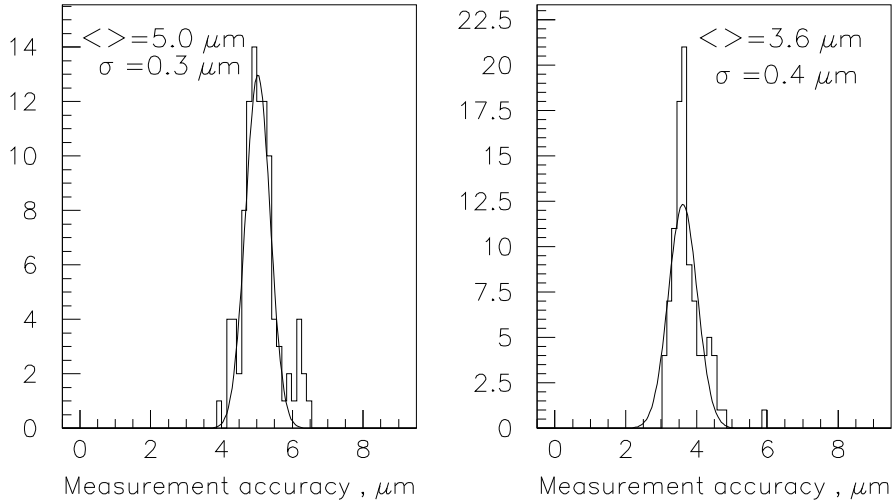

Figure 33: Measurement accuracies for the measurements shown in Fig.32 (top plot and second plot from top).

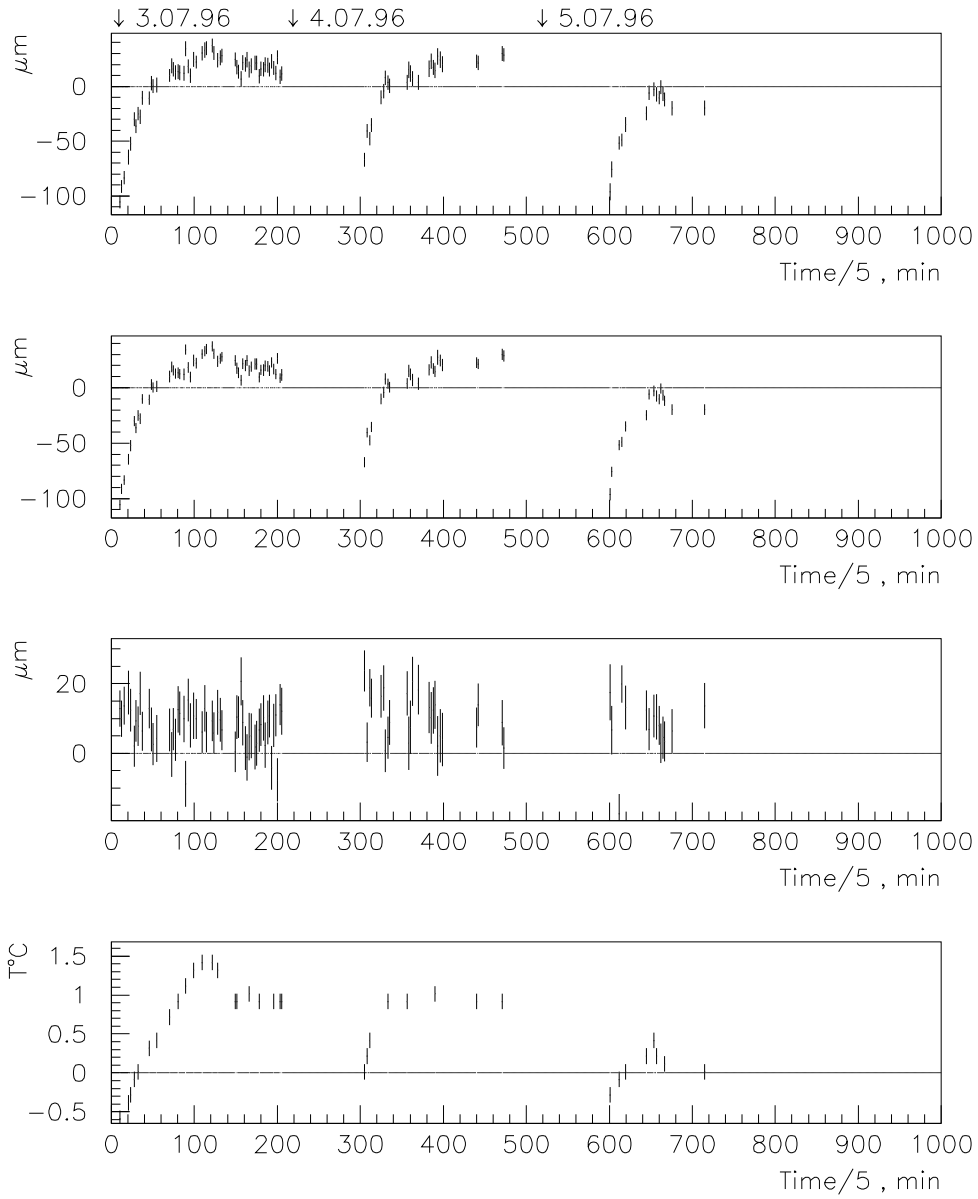

Figure 32: Variations of the measured wire positions caused by temperature fluctuations, for two wires (topmost and second topmost plots) as a function of time. The bottom plot shows the measured variations of the temperature itself, and the second plot from the bottom shows the variations in time of the distance between the two wires.

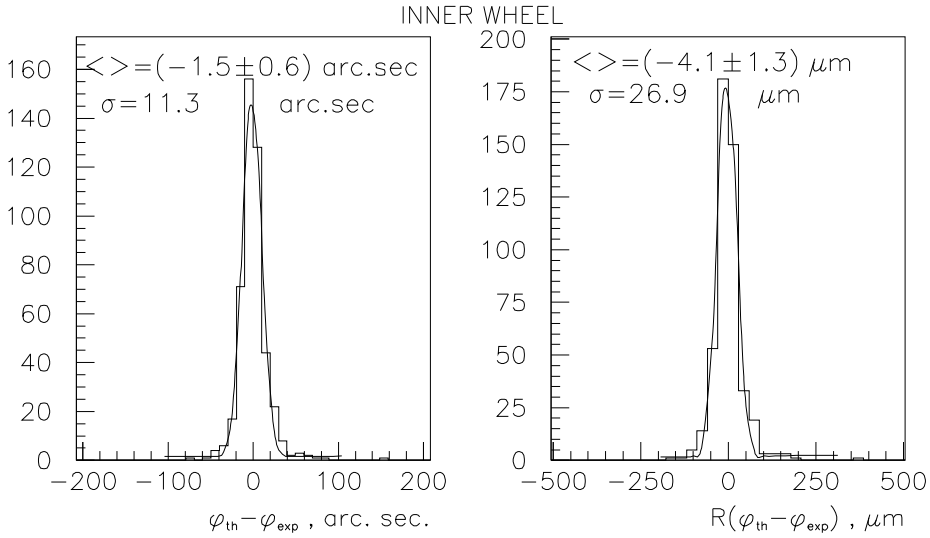

Figure 30: Difference between the measured and theoretical angular positions of the wire (left) and distance between these (right) at the radius of the inner wheel (R=0.5 m). Wires with $\varepsilon \geq 5\%$ have been excluded, in contrast to Fig.20.

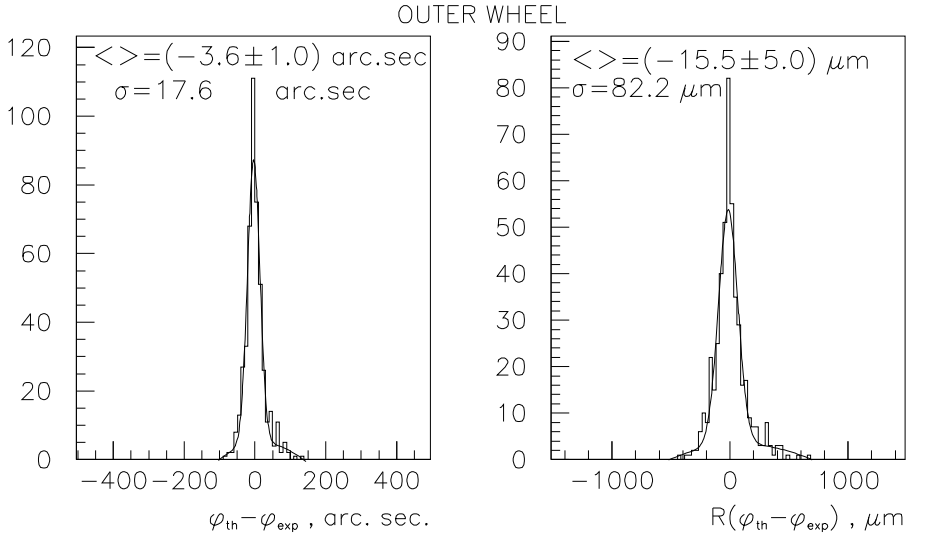

Figure 31: Difference between the measured and theoretical angular positions of the wire (left) and distance between these (right) at the radius of the outer wheel (R=1.0 m). Wires with $\varepsilon \geq 5\%$ have been excluded, in contrast to Fig.22.

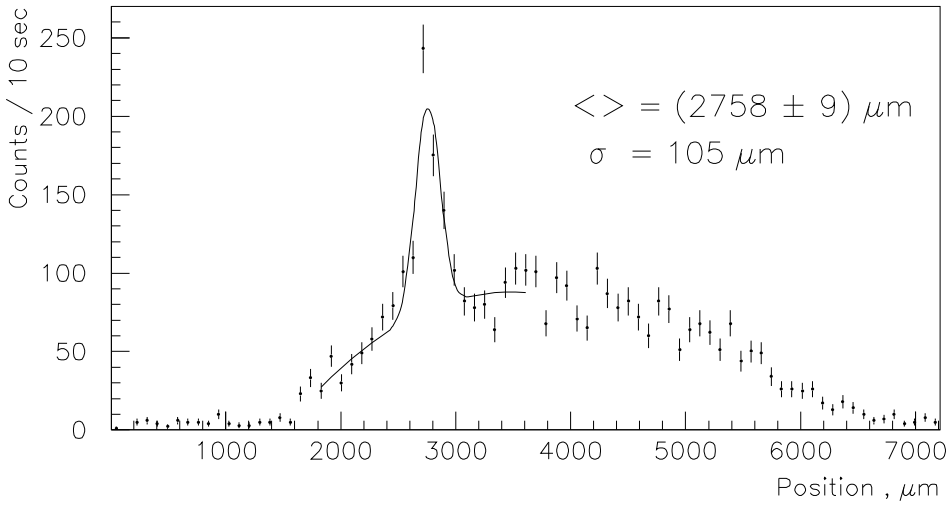

Figure 28: Same as Fig.24 for $\varepsilon \sim 50\%$.

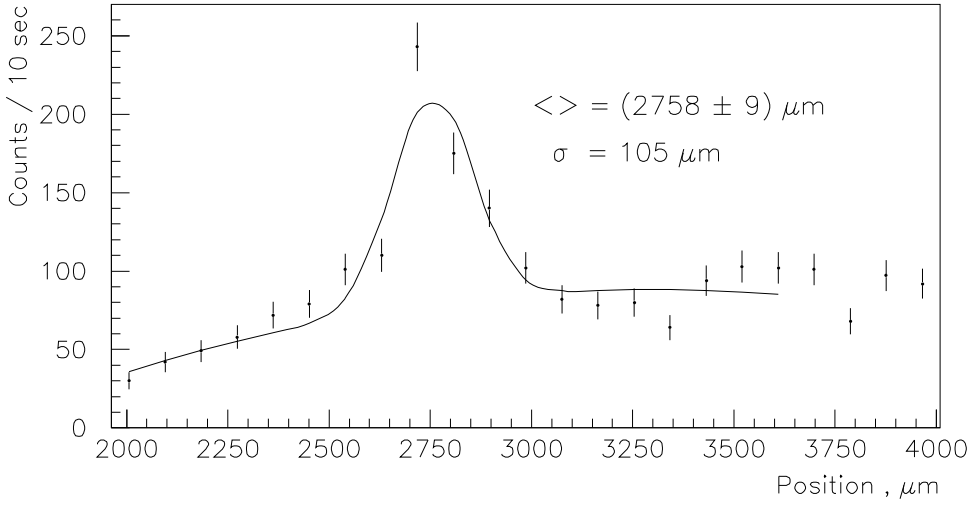

Figure 29: Enlarged wire profile for straw shown in Fig.28.

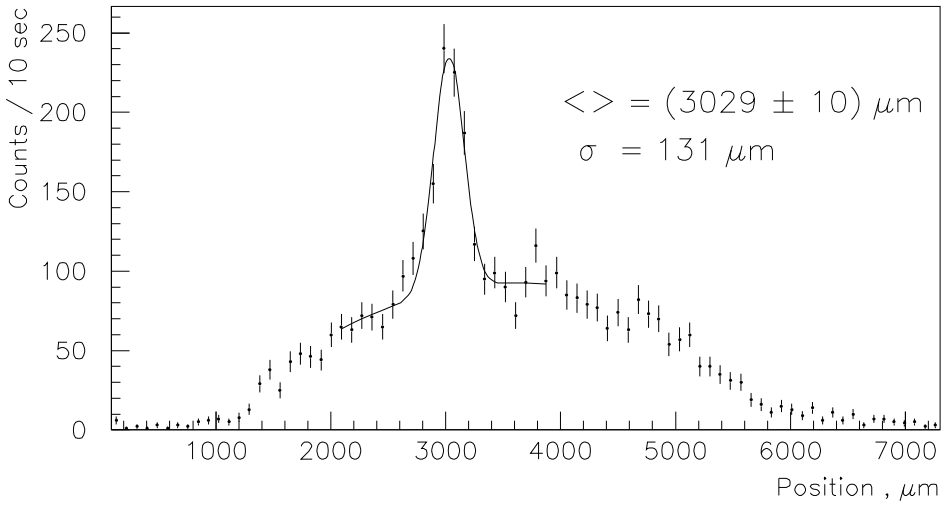

Figure 26: Same as Fig.24 for $\varepsilon \sim 20\%$.

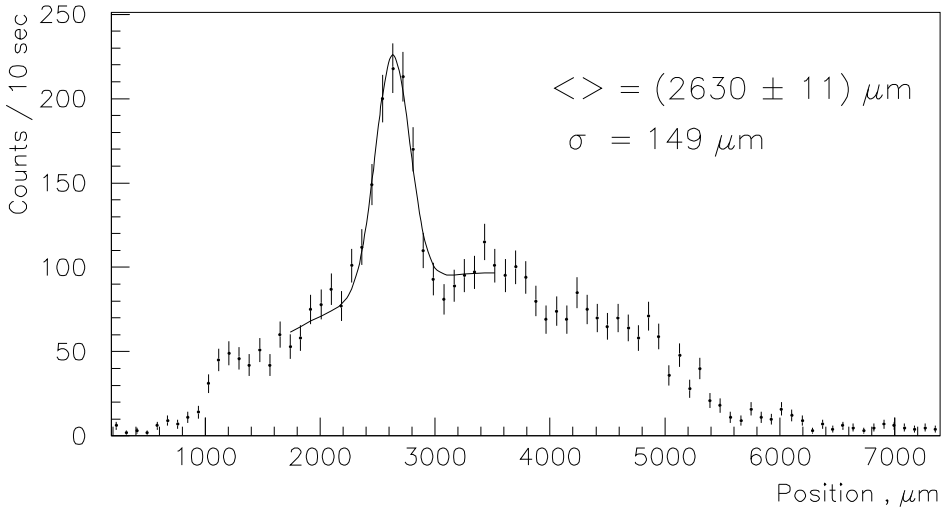

Figure 27: Same as Fig.24 for $\varepsilon \sim 35\%$.

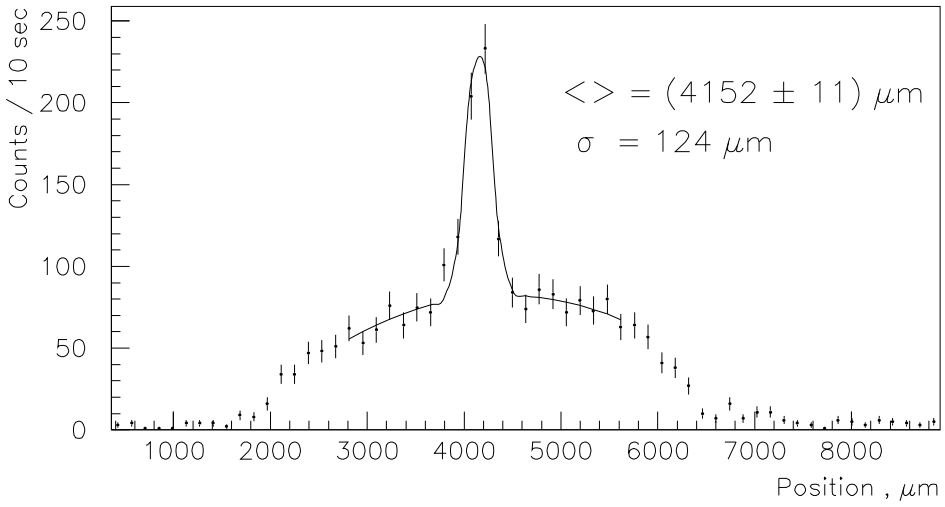

Figure 24: Example of measured straw profile for a wire eccentricity $\varepsilon \sim 7\%$.

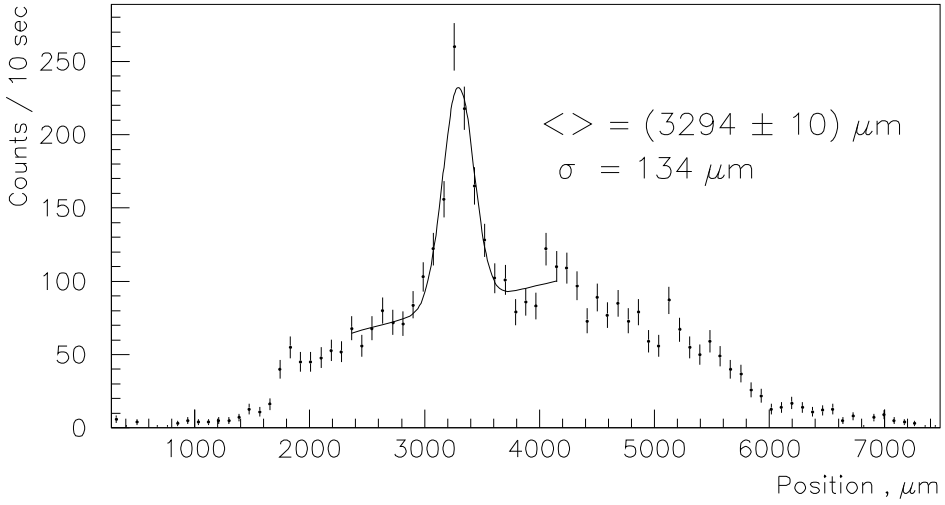

Figure 25: Same as Fig.24 for $\varepsilon \sim 12\%$.

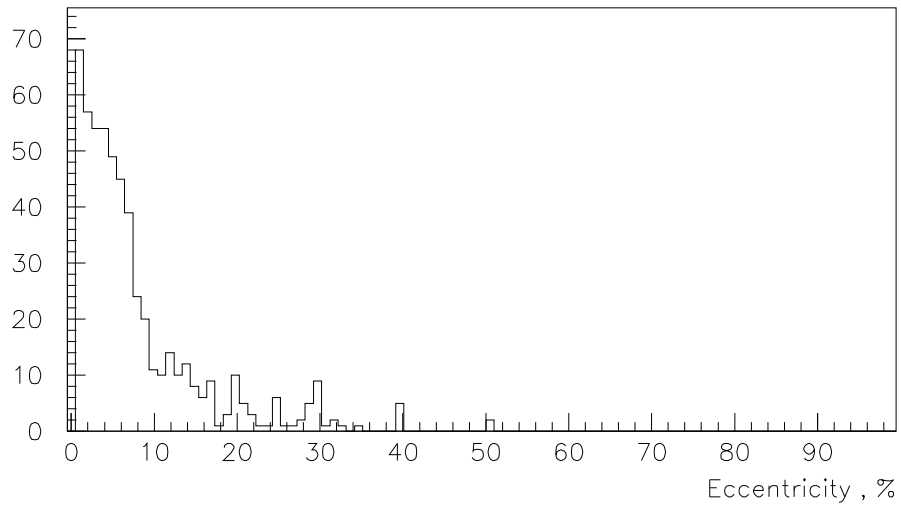

Figure 23: Measured eccentricity of the wire inside the straw as obtained using an Fe^{55} source.

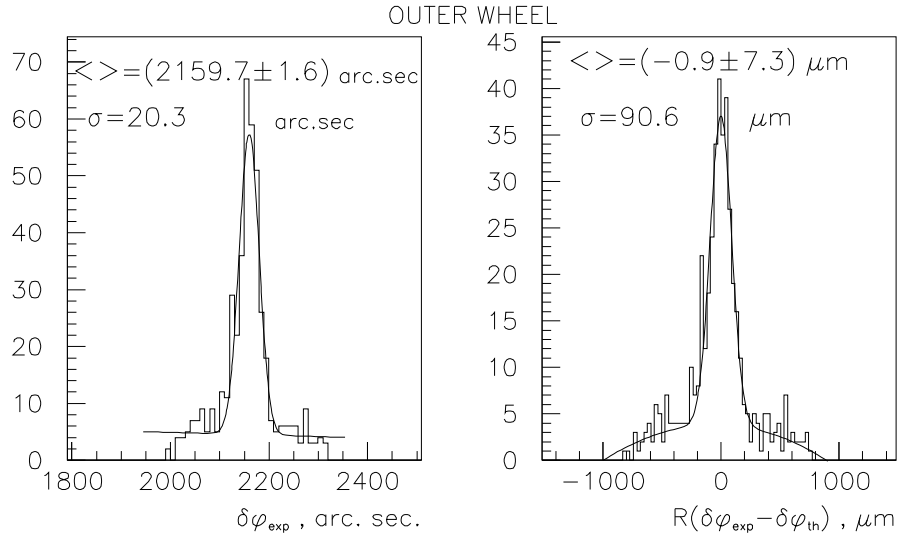

Figure 21: Difference between the measured angular positions for pairs of adjacent wires (left) and distance between these wires (right) at the radius of the outer wheel (R=1.0 m).

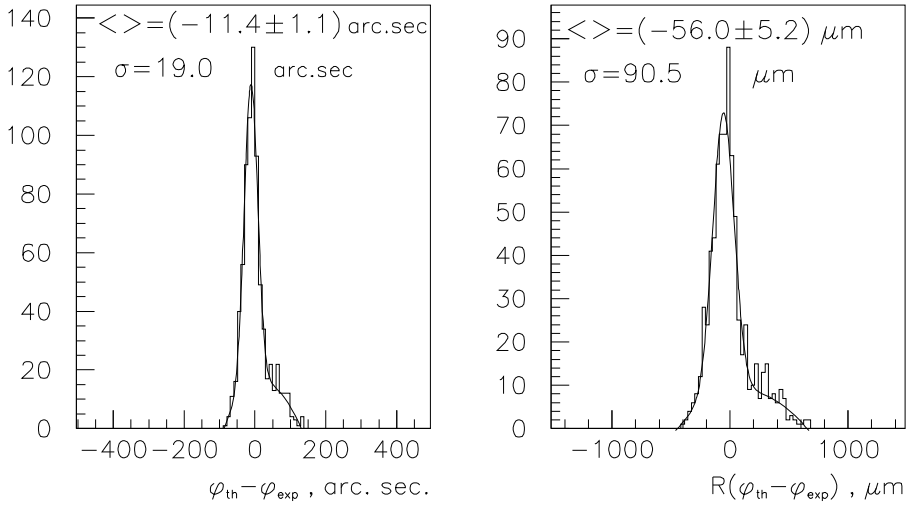

Figure 22: Difference between the measured and theoretical angular position of the wire (left) and distance between these (right) at the radius of the outer wheel (R=1.0 m).

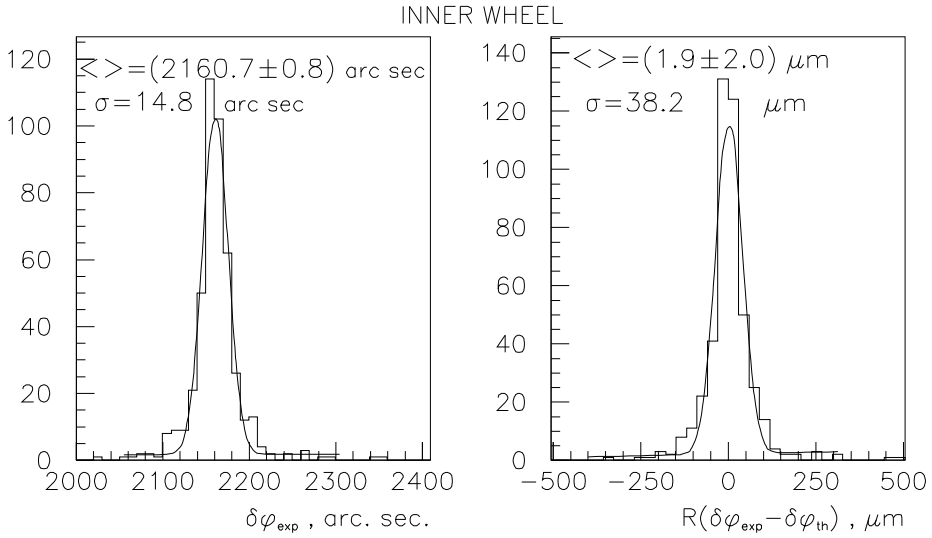

Figure 19: Difference between the measured angular positions for pairs of adjacent wires (left) and distance between these wires (right) at the radius of the inner wheel (R=0.5 m).

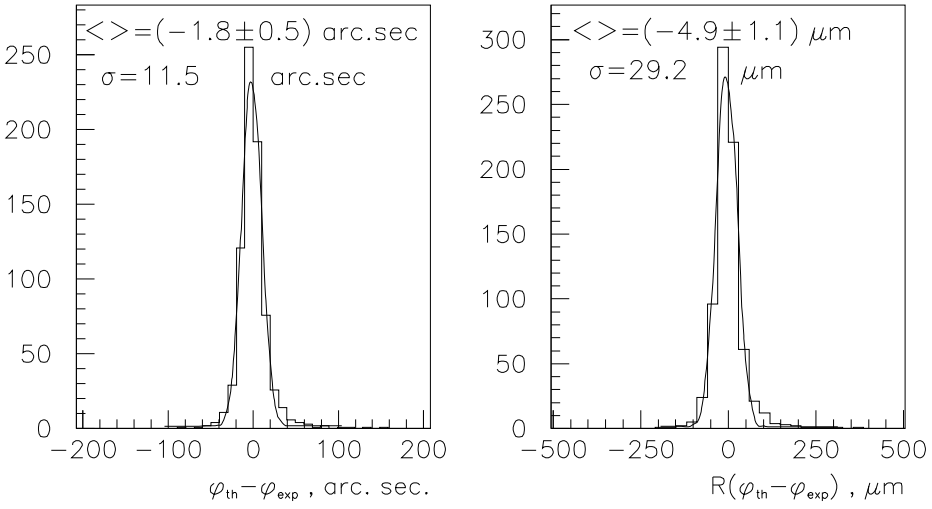

Figure 20: Difference between the measured and theoretical angular position of the wire (left) and distance between these (right) at the radius of the inner wheel (R=0.5 m).

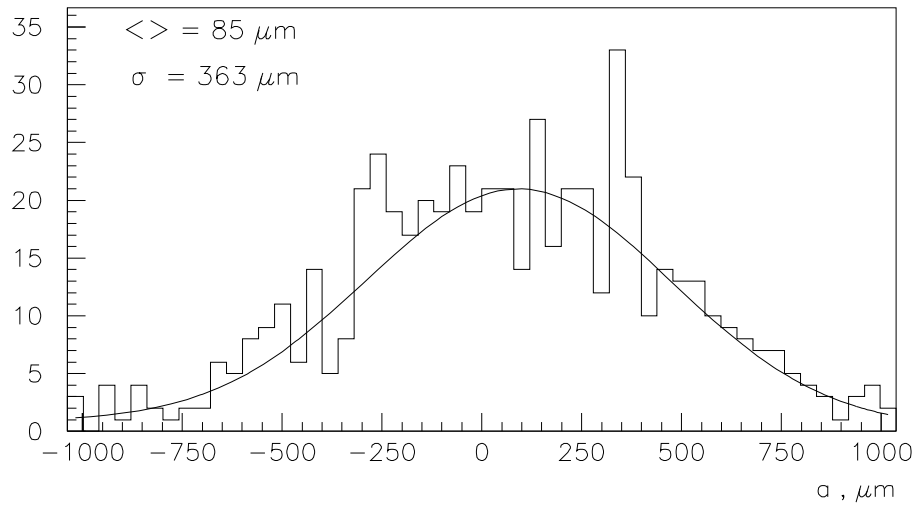

Figure 17: Distribution of values obtained for the parameter a described in Fig.3.

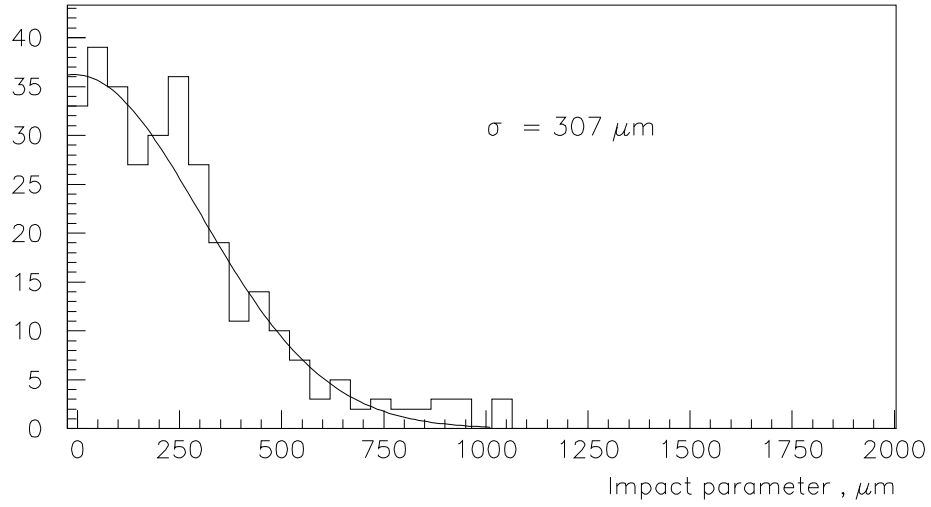

Figure 18: Measured impact parameter p in the X-Y plane (see Fig.3).

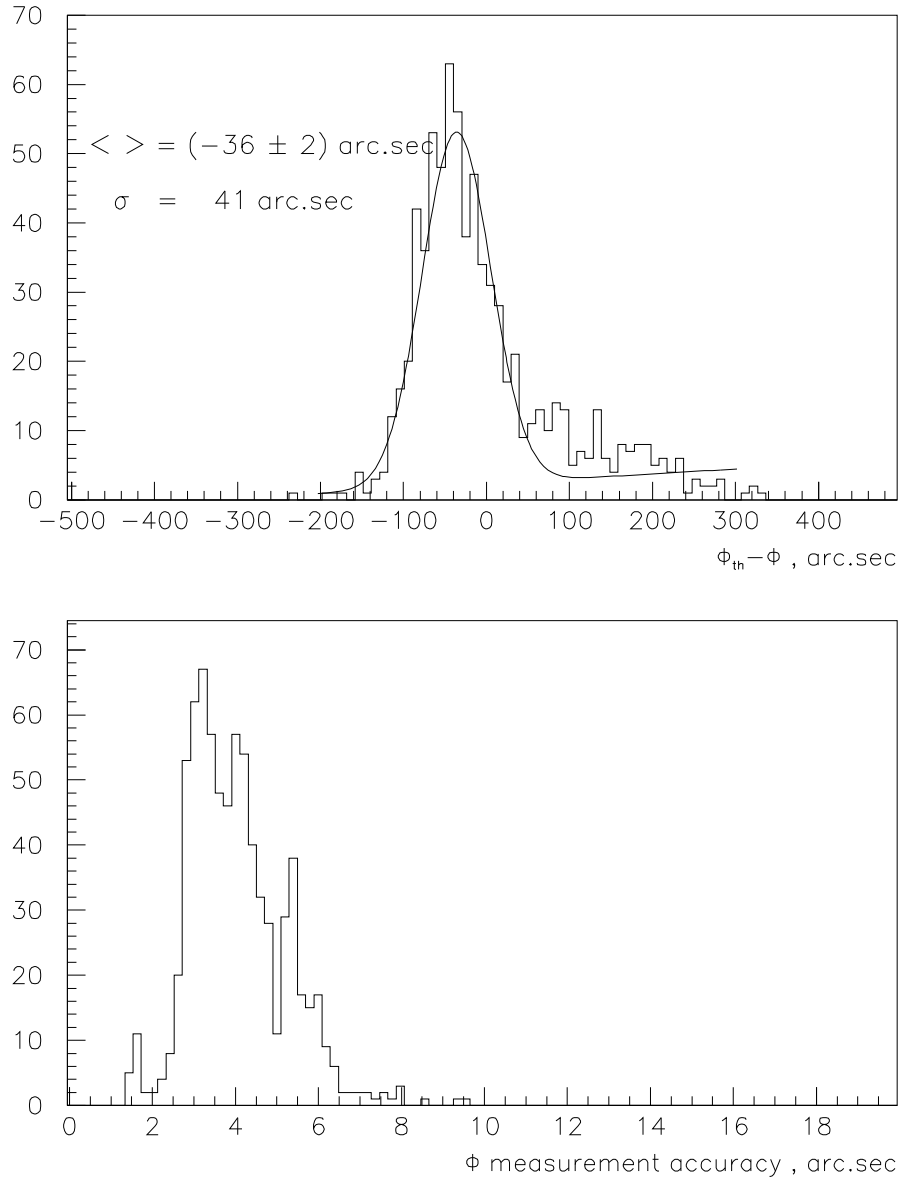

Figure 16: Distributions of the measured deviation of the parameter Φ defined in Fig.3 from is theoretical value Φ_{th} (top) and of the accuracy obtained on these measurements (bottom).

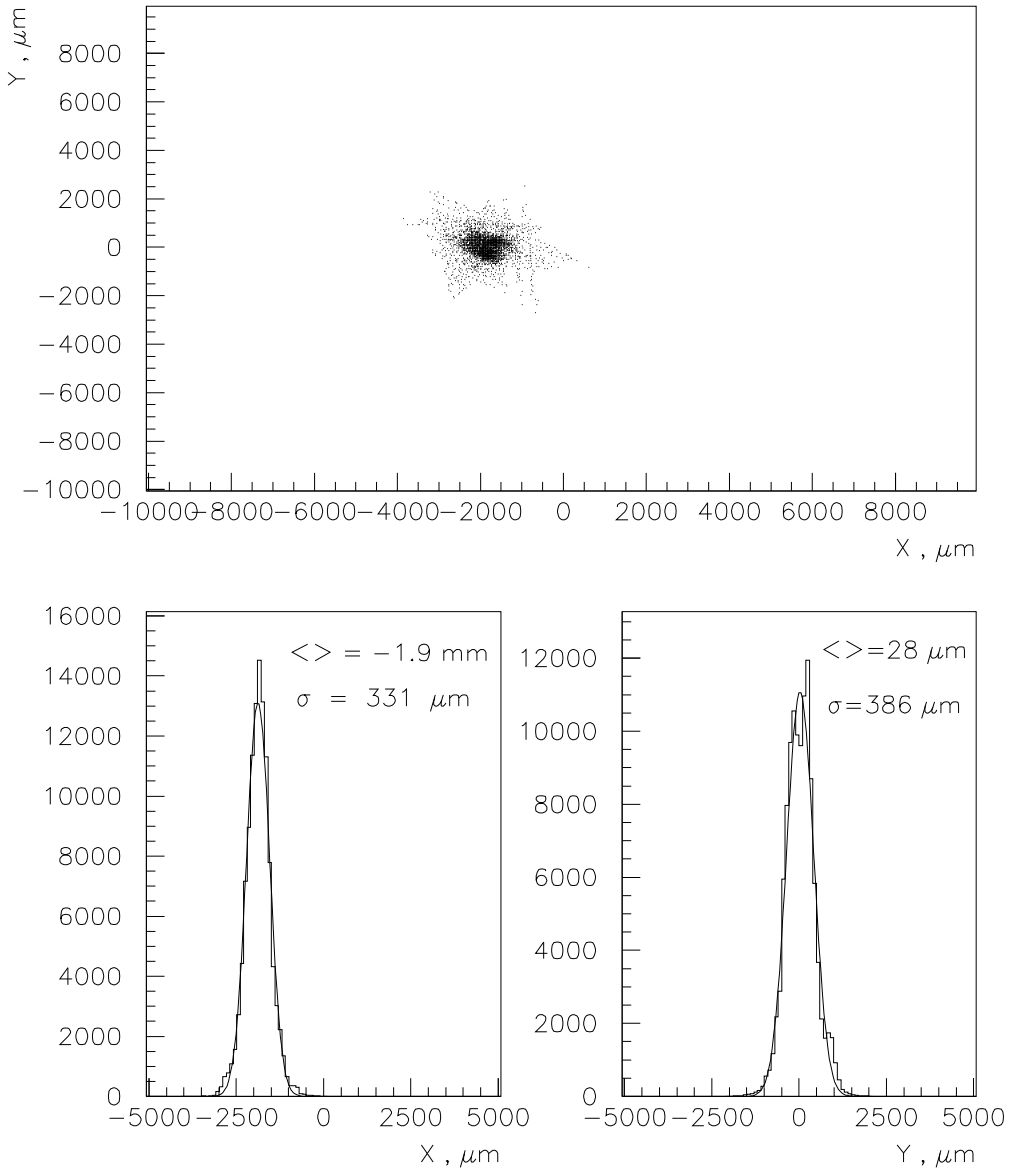

Figure 15: Two-dimensional plot of the coordinates of the intersection points between all wire pairs (top). Also shown are the projections of this plot onto the X-axis (bottom right) and the Y-axis (bottom left).

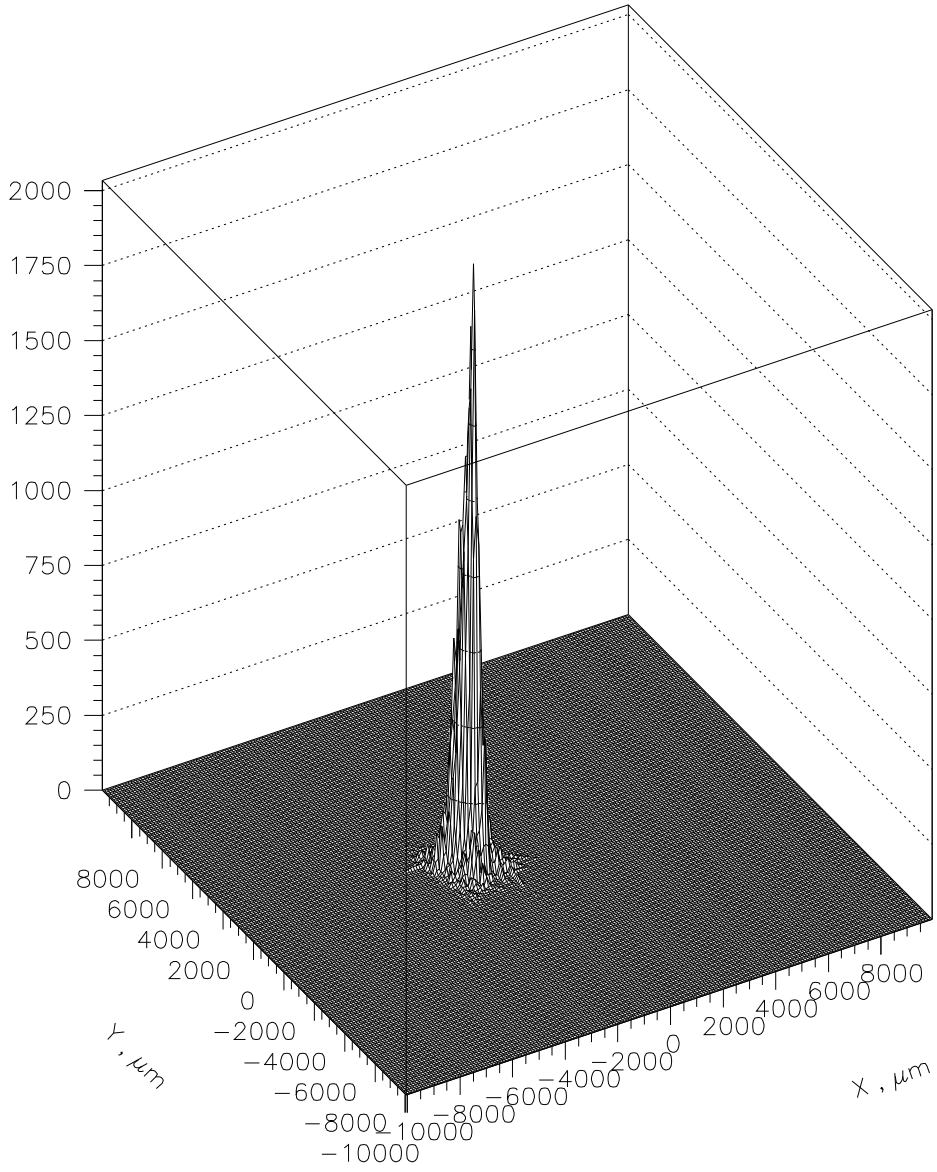

Figure 14: Three-dimensional plot of the coordinates of the intersection points between all wire pairs.

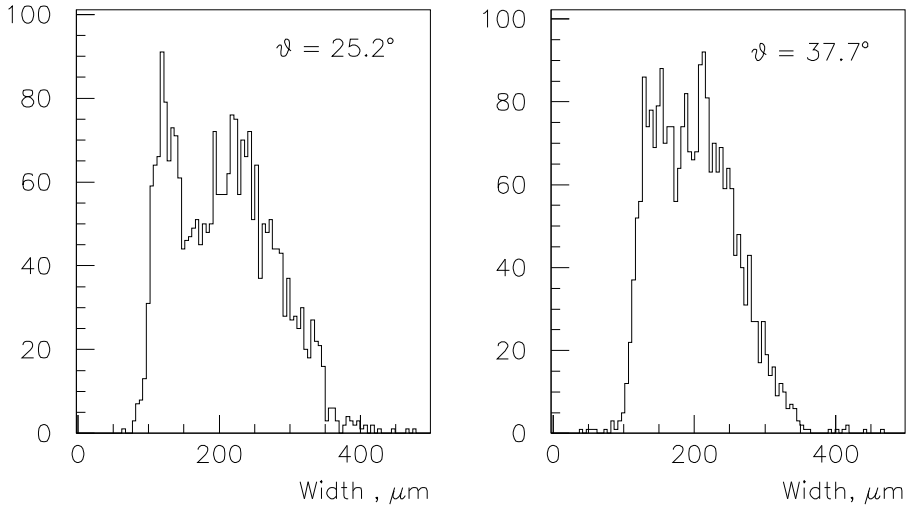

Figure 12: Measured total widths of the wire profiles for the two values of the elevation angle ϑ.

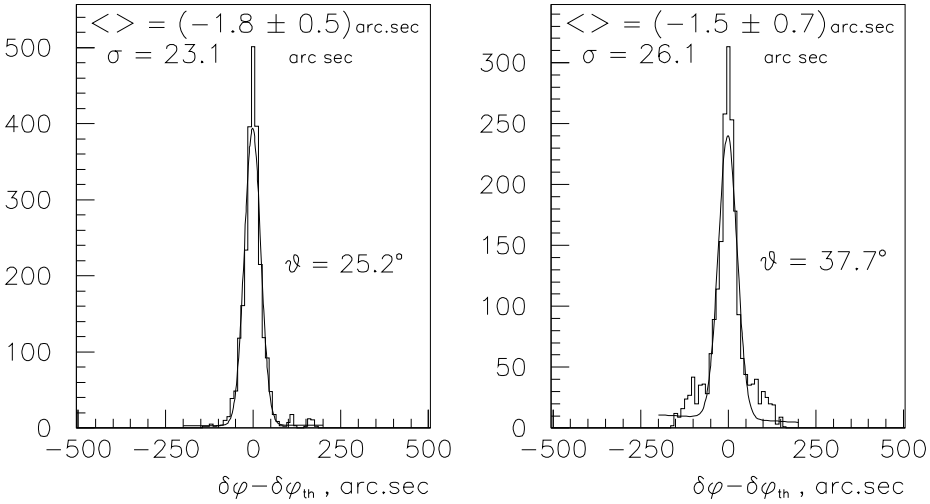

Figure 13: Deviations of the measured angle between pairs of adjacent wires from its theoretical value for the two values of the elevation angle ϑ.

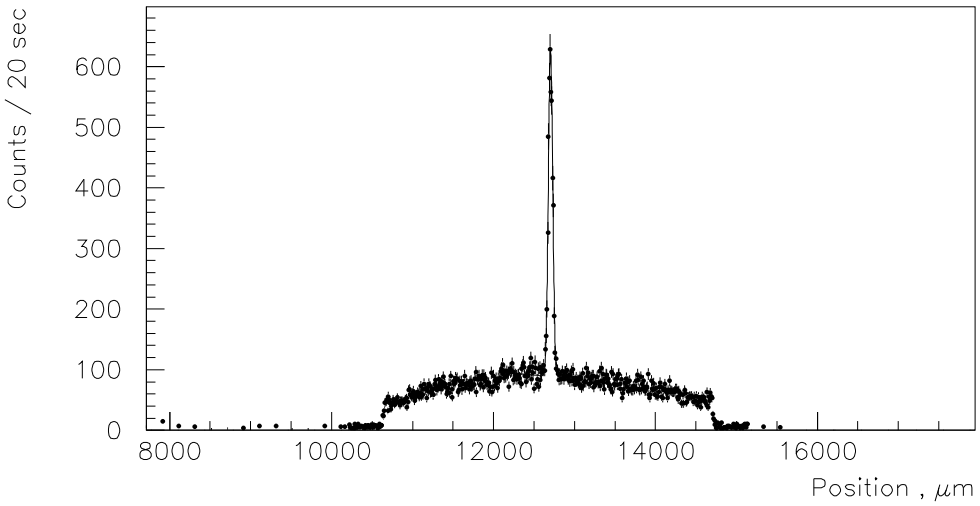

Figure 10: Measured straw profile in the best case of almost perfect parallelism between the X-ray beam and the wire; the straw profile has a total width close to the actual straw diameter of 4 mm.

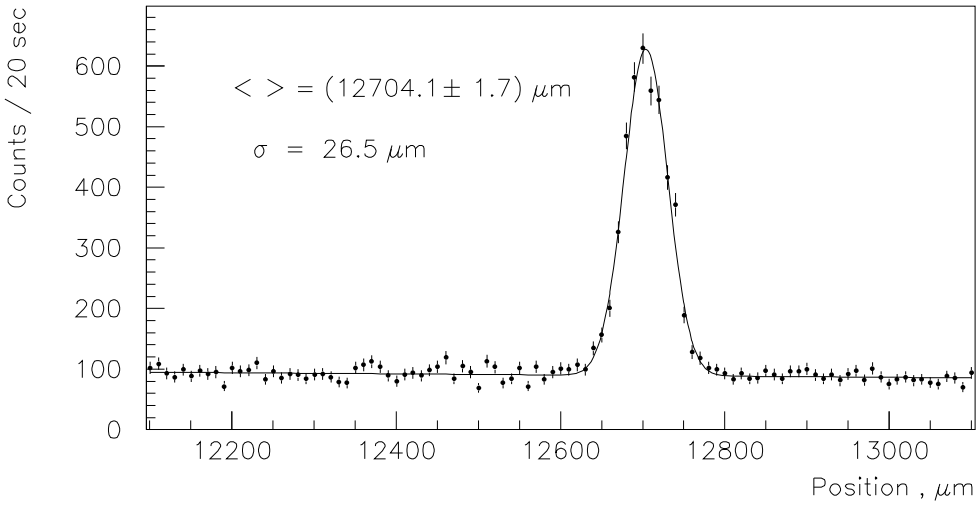

Figure 11: Measured wire profile for the case of Fig.10; the wire profile has an r.m.s. of 27 μm.

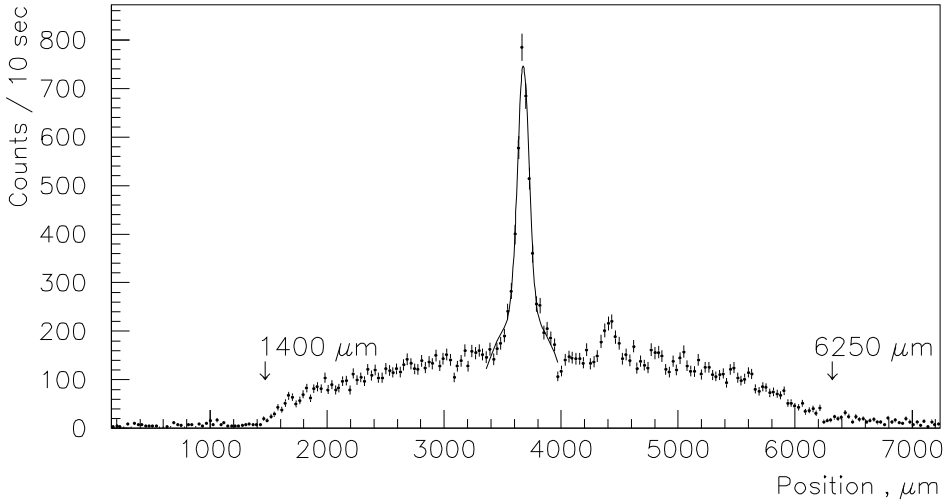

Figure 8: Measured straw profile in the case of imperfect parallelism between the X-ray beam and the wire; the straw profile has a total width of 4.8 mm.

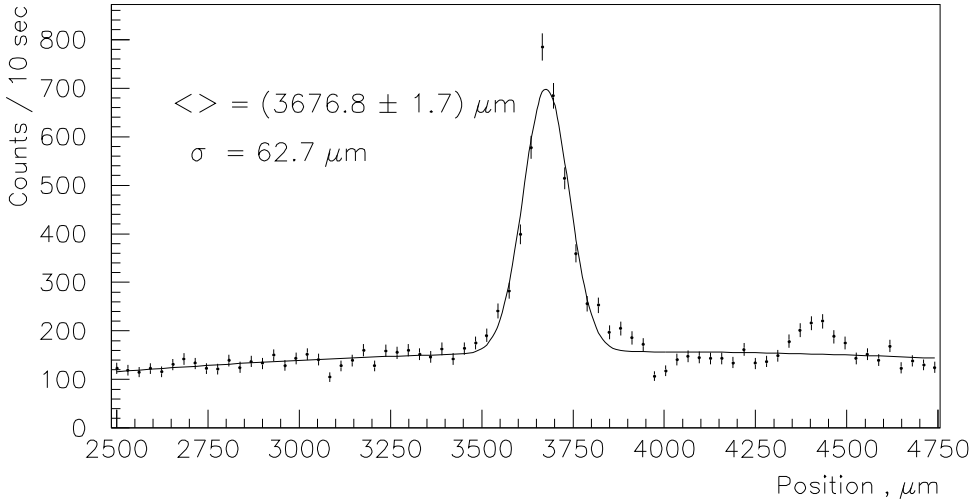

Figure 9: Measured wire profile for the case of Fig.8; the wire profile has an r.m.s. of 63 μm.

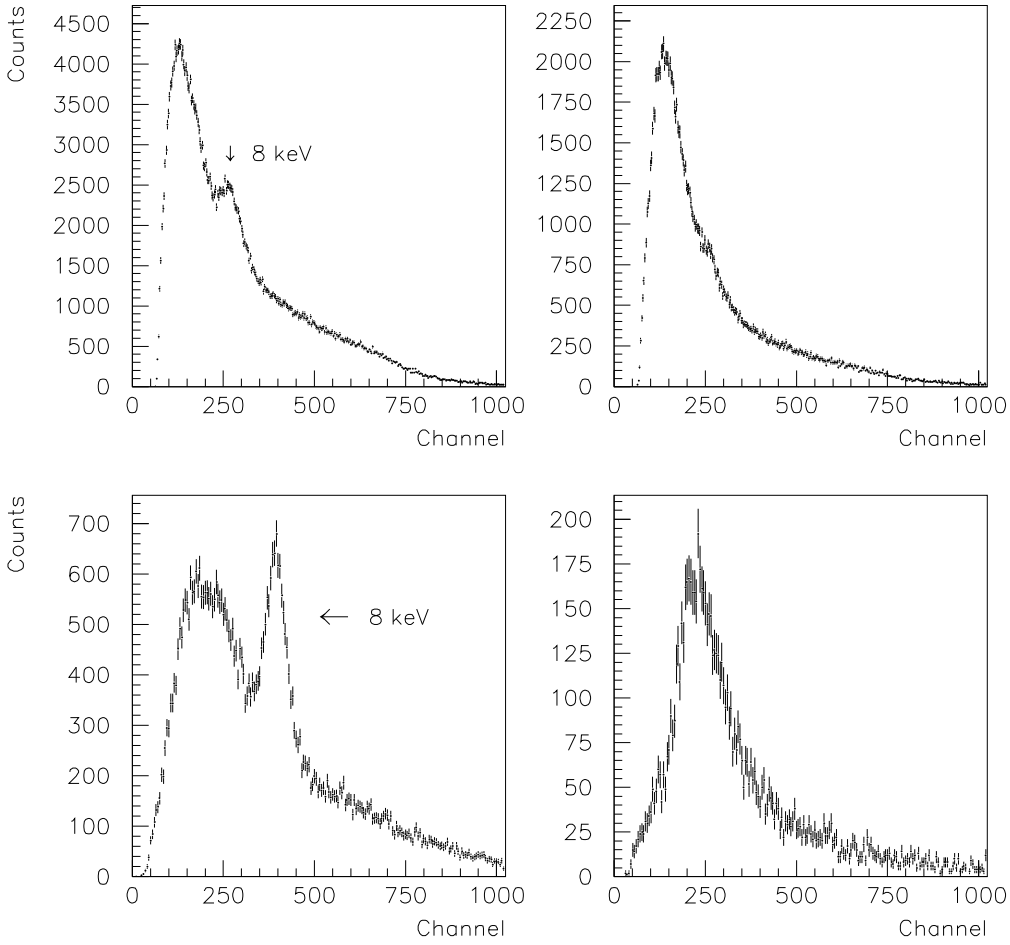

Figure 7: Amplitude spectra of the observed signal from the straw tube, if the X-ray beam irradiates the wire (left-hand plots) and if the X-ray beam only irradiates the gas (right-hand plots). The top plot corresponds to the general situation when the X-ray beam and the wire projection were not perfectly parallel. The bottom plot corresponds to the best case when the X-ray beam was almost perfectly parallel to the wire projection and the width of the X-ray beam was therefore equal to the wire diameter.

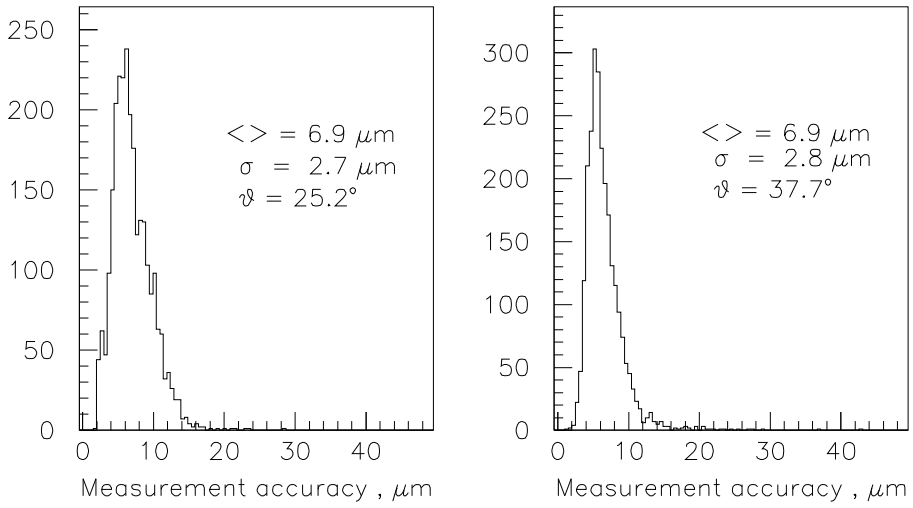

Figure 5: Estimated accuracies of the wire-position measurements for all measured wires and for the two values of the elevation angle ϑ.

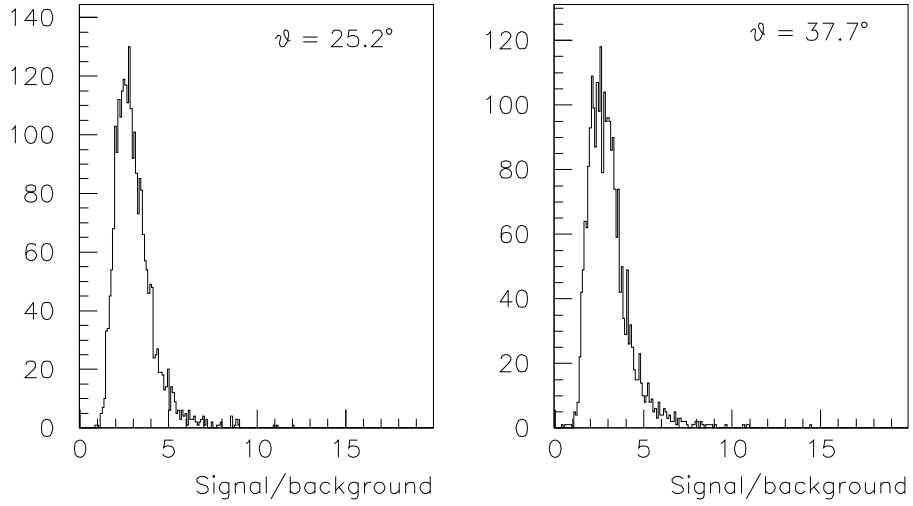

Figure 6: Ratio between counting rates when the X-ray beam irradiated the wire (signal) and when the X-ray beam only irradiated the gas (background), for all measured wires and for two values of the elevation angle ϑ.

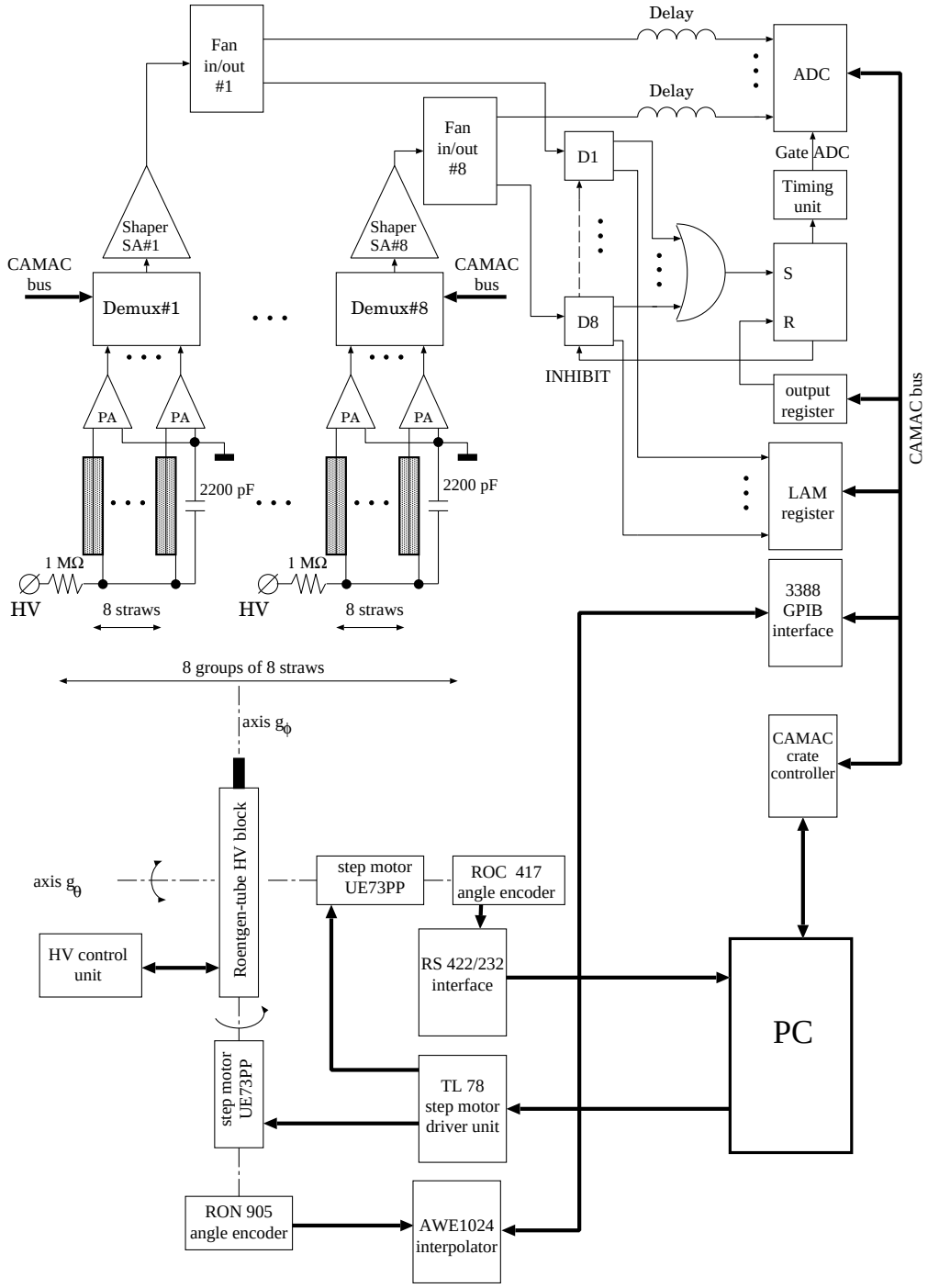

Figure 4: Schematic layout of the BDD control electronics and of the endcap TRT wheel prototype readout electronics.

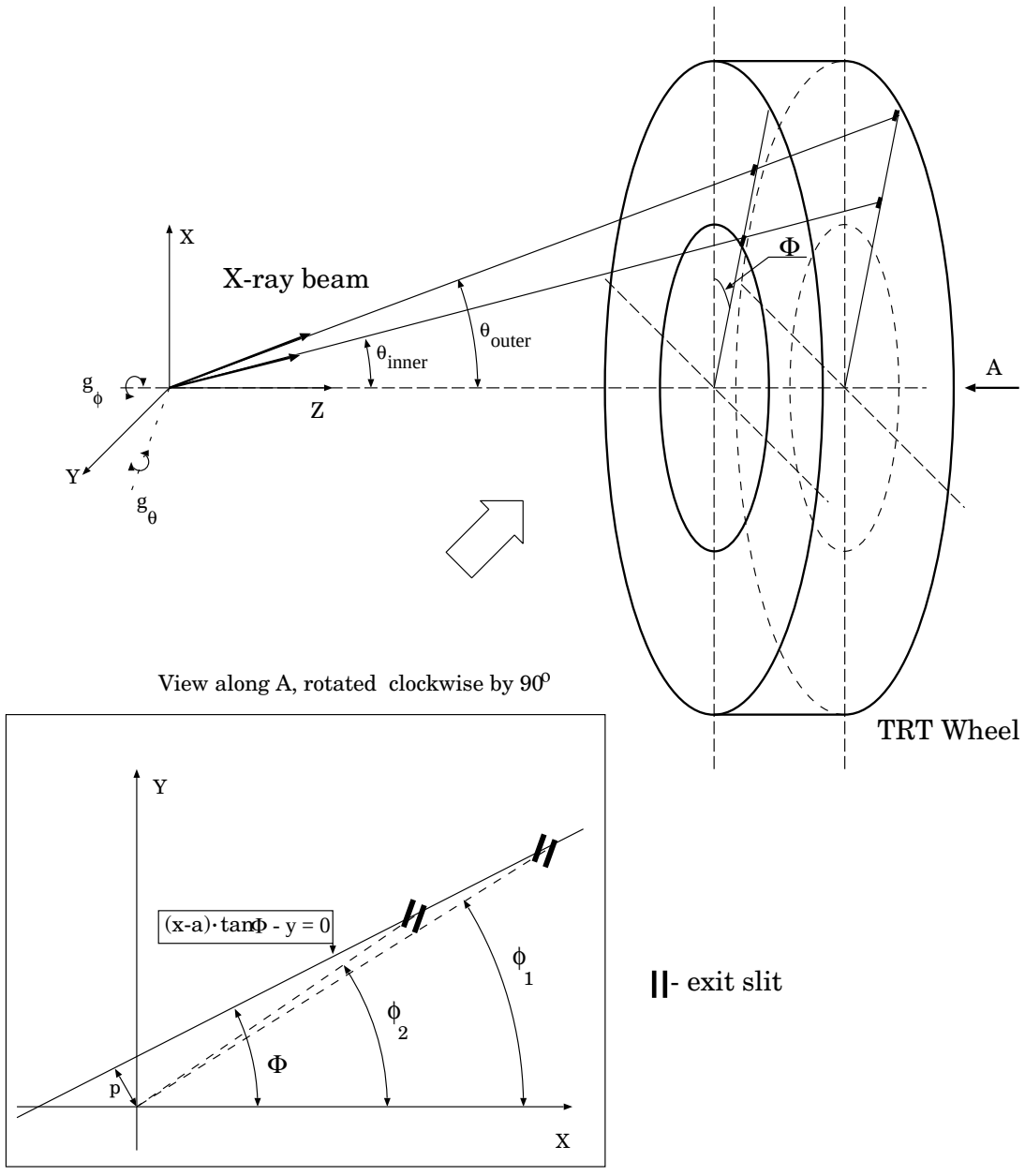

Figure 3: Illustration explaining the principle of the wire-position measurement by the BDD for the endcap TRT wheel prototype. Each wire is parametrised as a straight segment following the equation $(x-a)\tan\Phi - y = 0$ and p is the impact parameter of this straight segment with respect to the centre of coordinates.

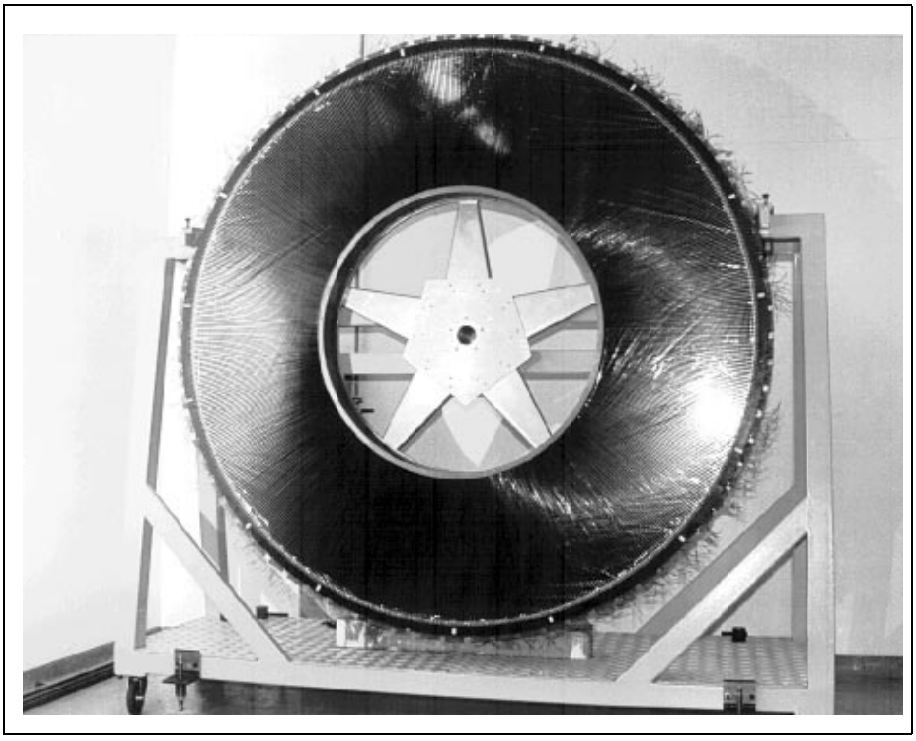

Figure 1: Photograph of the full-scale endcap TRT wheel prototype.

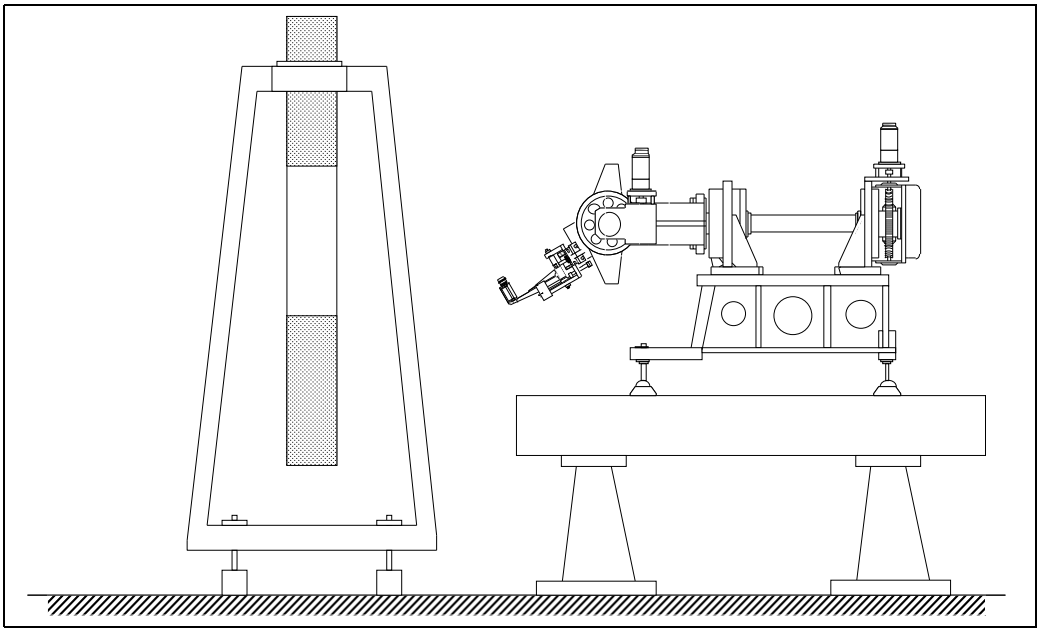

Figure 2: Side view of the Beam Directing Device installed in front of the endcap TRT wheel prototype for wire-position measurements using the X-ray beam.

List of Figures

References

[1] V. Ivanov, O. Fedin, A. Jelamkov, S. Muraviev, Yu. Platonov, A. Smirnov, An X-ray Measurement Station for the ATLAS Endcap TRT Calibration, Part 1: Design, adjustment and testing, ATLAS Internal Note, INDET-No-161 (1997).

[2] O. Fedin, S. Muraviev, A. Smirnov, First results of a TRT cell prototype alignment test with a 36 KeV X-ray beam, ATLAS Internal Note, INDET-No-057 (1994).

[3] R. Baum, D. Bernier et al., RD6 Collaboration : Manufacturing of the Endcap TRT Wheel prototype, Technical Note TA1/94-26, ATLAS Internal Note, ATLAS INDET-No-78 (1994).

[4] S.Muraviev et al., Tests of the Endcap TRT Wheel, ATLAS Internal Note, (1997), to be published.

cantly broader than expected, and the signal-to-background ratio in terms of counting rate was decreased from the ideal value of 6:1 to about 3:1.

In summary, the time necessary for a complete measurement of such a wheel, containing 9600 straws, can be estimated to be at least 320 hours of continuous work, provided the exposure time per measurement can be decreased to two seconds, one second for the measurement itself and one second for the movement of the BDD to the next point. Each wire profile would consist of 30 measurement points taken for two values of the elevation angle ϑ. The calibration time may also be reduced by optimising the X-ray energy, since the choice of 36 keV may not be optimal for this particular detector.

The measurement of the wire-positioning accuracy was obtained from pairs of adjacent wires and also by comparing each measured wire position to its predicted one, both at the radius of the inner and outer wheels. Of 752 wires retained for further analysis, 32 wires (i.e. 4.3%) were found to be outside the overall tolerance of ± 100 μm foreseen for the final design at the radius of the inner wheel. In contrast, as many as 118 (16%) were found to be outside ± 250 μm at the outer radius. Even though this proportion drops to 8% when eliminating wires which were incorrectly fixed at the outer radius, more work will clearly be needed in the final design phase to achieve the required tolerance of ± 100 μm at the outer radius as well.

For most of the wires, however, these measurements have shown that the engineering design and manufacturing of the structures was a success, since the wire positioning accuracy was measured to be 30 μm at the inner radius and 80 μm at the outer radius.

support, the endcap TRT wheel prototype and its support structure, was not in a temperature-controlled environment, and the support structures were not designed for optimal temperature stability. Nevertheless, two wires, distant by ~ 8 cm, were measured regularly by the X-ray beam over a period of three days, during which the temperature was continuously monitored. As shown in Fig.32, the measured wire positions varied by up to ~ 150 μm for an overall excursion of $\sim 2^o$ in temperature. The distance between the two wires was measured to be stable to better than 30 μm, and Fig.33 shows that the individual measurement accuracies were all around 5 μm. The conclusion from the results in Fig.32 is clearly that a few straightforward improvements in the mechanical stability of the support structures of both the BDD and the wheel would be needed to achieve a better reproducibility of the measurements over periods of days.

7 Conclusions

The results presented in this note demonstrate that the positions of the individual wires inside the straws of the endcap TRT wheel prototype can be measured automatically with the X-ray beam to an accuracy of better than 10 μm in the absence of systematic effects which could be due in particular to temperature variations. This accuracy was entirely determined by the statistical accuracy of the measurements.

Though the intensity of the X-ray beam was initially increased by a factor two by a careful adjustment of the X-ray monochromator, the time necessary to achieve the required statistical accuracy remained unchanged for the following two reasons:

- the imperfect parallelism between the wide component of the X-ray beam and the wire projection, mainly due to the fact that the exit slit of the monochromator was not perfectly perpendicular to the g_ϑ-axis of rotation; because of this, the time per measurement point had to be increased twofold, since it turned out to be necessary to repeat all measurements after rotating the BDD around the g_φ-axis by 180^o, which allowed the analysis procedure to effectively eliminate systematic errors due to this effect;

- the imperfect alignment of the BDD with respect to the centre of the wheel. As a consequence, many of the wire profiles were measured to be signifi-

adjacent holes at radii of 0.5 m (Fig.19 right) and 1 m (Fig.21 right). The r.m.s. values of these distributions are 38 μm and 91 μm respectively. The positioning accuracy of both wires in the pairs considered contributes to these r.m.s. values. A more direct measurement of the individual wire positioning accuracy is shown in Figs.20 and 22 respectively for the inner and outer wheels. The r.m.s. values of these distributions, respectively 29 μm and 91 μm, reflect the overall mechanical accuracy achieved in positioning the wires. The expected mechanical accuracies were very similar, $\sim$ 30 μm at both radii, in the original design. However, due to the introduction at a later stage of carbon-fibre reinforcements glued to the straws, as mentioned in Section 2, this mechanical accuracy could not be achieved by design at the outer radius.

Another noticeable difference between Figs.20 and 22 is the presence of significant and asymmetric non-Gaussian tails in Fig.22. These tails are explained as wires inaccurately fixed at the outer radius during the stringing procedure, due to faulty fixation pins. The tail is asymmetric because the stringing procedure and wire-guide design only allowed errors in wire positioning in one direction.

This effect was investigated by measuring directly the wire eccentricity inside the straw through variations of the measured signal amplitude from a Fe^{55} source along the length of the straw. The wire eccentricity was defined as the relative maximum amplitude excursion measured, $\varepsilon = \frac{A_{max}-A_{min}}{A_{mean}}$, where A_{max} and A_{min} were respectively the maximum and minimum measured amplitudes along the straw length. Fig.23 shows the distribution obtained for this ε, which is in most cases less than 10%.

For eccentricities larger than 5-10%, the wire is more than 300 μm away from the centre of the straw, and the X-ray measurements confirm this earlier experimental observation [4], as shown in Figs.24 to 29. In fact, the correlation between the X-ray measurements and the direct wire eccentricity measurements is shown to be excellent in Figs.24 to 29.

The measured values of the wire eccentricity were used to exclude the badly installed wires from the analysis of the X-ray measurements. Only wires with $\varepsilon < 5\%$ were retained and the results for these are shown in Figs.30 and 31. The r.m.s. values have slightly improved compared to Figs.20 and 22 for both distributions to 27 μm and 82 μm respectively, but the main effect which is observed is the disappearance of most of the large asymmetric tail which is present in Fig.22.

Finally, the temperature stability of these measurements has been checked carefully, as illustrated in Fig.32. The overall system, including the BDD, its

for the two values of the elevation angle ϑ. On average the total width is found to be $\sim$200 μm, significantly larger than the ideal value of $\sim$120 μm (see Fig.11). The distributions in Fig.12 display two peaks, one close to the ideal position of $\sim$120 μm , the other one around 230 μm. This can be explained, if one assumes that the intersection point between the g_φ-axis of rotation of the BDD and the plane of the wheel does not coincide exactly with the centre-of-symmetry of the wheel. In an attempt to find the position of this centre-of-symmetry of the wheel, the coordinates of the intersection points between all measured wire pairs were calculated and plotted in Figs.14 and 15. A clear displacement of $\sim$ 1.9 mm in the vertical direction (X-axis) is observed, whereas in the horizontal direction this displacement is measured to be only $\sim$ 30 μm. As can be seen from Fig.15, the r.m.s. of the projections are $\sim$ 350 μm in both directions, and the large displacement observed in the vertical direction is most probably due to the difficulty of adjusting the position of the wide component of the X-ray beam.

The design value required by construction for the angle between two adjacent wires is $\delta\varphi_{th} = 2160''$. Fig.13 shows the differences between the measured value $\delta\varphi$ of this angle and $\delta\varphi_{th}$, for all pairs of adjacent wires which were measured and for both values of the elevation angle ϑ. The measured values agree with the design figure to better than $2''$ for both values of the elevation angle ϑ.

The next step in the analysis was to extract the individual wire parameters from the measurements, i.e. the parameters Φ, a and p described in Fig.3, which characterise the straight line segment representing the wire in the X-Y plane. Fig.16 shows the distributions obtained for the angle Φ (in terms of its deviation from its theoretical value Φ_{th}) and its error. After correction for the displacement of the centre of the BDD coordinate system with respect to the centre-of-symmetry of the wheel discussed above, the second parameter, a, describing the straight line segment representing the wire in the X-Y plane, and the impact parameter, p, of this straight line segment with respect to the centre of coordinates were extracted from the individual wire measurements and are shown in Figs.17 and 18.

The mechanical accuracy of the wire positioning inside the wheel can be extracted from the measurements by comparing the measured values of φ_1 and φ_2 (see Fig.3) to the theoretical positions of the centres of the holes in each support ring at radii of 0.5 and 1.0 m. As shown in Figs.19 and 21 for the inner and outer wheel respectively, a first indication of this accuracy can be simply obtained by transforming the results shown in Fig.13 for the angular distance between adjacent wires into distributions of the distance in μm between two

the elevation angle ϑ_{inner} and ϑ_{outer} mentioned previously. The complete set of measurements for a given wire thus yielded two azimuthal angular positions φ_1 and φ_2, and two additional ones φ_1' and φ_2' obtained after rotating the BDD by 180^o around the g_φ-axis.

Fig.5 shows the estimated accuracies of all wire-position measurements for the two values of the elevation angle ϑ. Most wires were measured with an accuracy better than 10μm. The peaks in Fig.5 are at a position of $\sim 7\mu$m, a value which depends almost entirely at this level on the time allocated to each measurement. The exact shape of the distributions in Fig.5 is strongly correlated to the distribution of the ratio of measured counting rates for the X-ray beam irradiating the wire (signal) and only irradiating the gas (background). The distributions of this signal-to-background ratio are shown in Fig.6: they depend strongly on the degree of parallelism achieved between the wide component of the X-ray beam and the measured wire itself[4]. In the optimal case of perfect parallelism, the projected width of the X-ray beam perpendicular to the wire is of the order of the wire diameter and the signal-to-background ratio is about 6:1. Due to the imperfect parallelism achieved in real measurements, this ratio was on average about 3:1, as shown in Fig.6.

The impact of this imperfect parallelism can also be directly seen in the measured amplitude spectra, as shown in Fig.7. This figure shows the measured amplitude spectra for the X-ray beam irradiating the wire (left) and only irradiating the gas (right), and for the general case of imperfect parallelism between the beam and the wire (top) and the rarer case of almost perfect parallelism (bottom). In the latter case, the 8 keV K_α-emission line of copper can be observed easily above the background from X-ray absorption in the gas.

Another consequence of this imperfect parallelism between the X-ray beam and the wire projection is a broadening of the measured wire and straw profiles. Fig.8 shows one example where the measured straw profile has a total width of ~ 4.8 mm, 20% larger than the actual straw diameter. The wire profile obtained for this straw is shown in Fig.9, and is also broader than expected with an r.m.s. of 63 μm. In contrast, Figs.10 and 11 show the same profiles in the case of almost perfect parallelism between the X-ray beam and the wire. These figures also show that, in this optimal case, a signal-to-background ratio of 6:1 is achieved.

Fig.12 shows the distributions of the measured total width of the wire profiles

[4]At a distance of $\sim$ 1.3 m, the X-ray beam has a size of 100 μm for the narrow component and of 130 mm for the wide component

RS-422/232 interface simplifies the RS-422 standard code to a RS-232 standard one. The accuracy of the ROC-417 is ± 1 bit, which corresponds to $10''$ ($48\ \mu$rad).

The rotations around the g_φ-axis, which have to be measured to a better accuracy, are encoded through an incremental angle encoder (RON905), which uses projected light scanning with transmitted light. The measuring standard for this encoder is a graduated glass disk with radial gradations consisting of 36000 lines and gaps on one track, while a second track carries one reference mark. The rotation of this disk modulates the light beam, and the transmitted light intensity is measured by photo-voltaic cells, which are connected to a circuit which outputs two sinusoidal incremental signals, phase-shifted by 90^o with respect to each other, and one additional signal peak corresponding to the reference mark. These sinusoidal output signals are 1024-fold interpolated and digitised in an interpolator (AWE1024). The measurement step is $\sim 0.036''$ and the accuracy is $0.4''$ after direct interpolation, improved to $0.2''$ ($1\ \mu$rad) after adjusting the amplitudes of the sinusoidal signals in a calibration run. A 3388-GPIB CAMAC interface converts the GPIB (General Purpose Interface Bus) standard to a CAMAC-compatible one.

The high-voltage (HV) control unit supplies the X-ray tube HV-block with a low voltage of 12-20V. The HV-block itself converts this voltage to a DC voltage of up to 100 kV and returns to the control unit the values of the tube current and voltage, which are digitised and displayed at all times.

6 Results of the measurements

Over a period of two months, 10 cells or 1280 wires of the wheel prototype were measured, thus sampling uniformly 10% of the wheel. For various reasons described in [4], about 28% of the straw wires could not be measured, and therefore only 921 wires were measured with the X-ray beam[3].

In a first step, the analysis of the measurement results was stored into a database and concentrated on eliminating inaccurate or incomplete measurements (bad signal-to-background ratio between wire peak and gas peak, measurement of poor quality). Only 752 wires were retained for the final analysis, corresponding to those which were accurately measured for the two values of

[3] A more complete discussion of the wheel design, measured straw signal properties, high voltage behaviour etc. can be found in [4] .

ϑ_{inner} and $10''$ in case of ϑ_{outer}.

The measured wire profiles were then fitted using an automatic procedure and the results from the fit (centre of gravity of the wire profile, amplitude and width of signal and background) were stored in a database. These data were then used to compute the parameters of the wire equation. The data presented in the next Section were fitted to a Gaussian shape (wire profile) plus a linear background (X-ray absorption in the straw gas). Although the shape of the wire profile is more complex than a simple Gaussian, this approximation was found to remain valid for the X-ray beam widths and wire diameters considered here.

5 Electronics

Fig.4 shows the electronics set-up used for the X-ray measurements. An analog circuit was used to record simultaneously the signals from 8 straws. Four preamplifier cards were equipped with 16 preamplifiers for two groups of 8 straws in two neighbouring layers. Every pair of layers equipped by preamplifiers was separated from the next equipped pair by one pair of empty layers. Camac-driven multiplexers selected the wires which were under irradiation by the X-ray beam and supplied their signals to a shaper. The shaped signals have a bipolar form with a rise-time of about 100 nsec. After shaping, the signals were discriminated and then after an additional delay, were sent to the inputs of an ADC. The gate for the ADC was produced by all signals with an amplitude exceeding the discriminator threshold. This threshold corresponded to an energy deposition in the straw of about 1-2 keV. After this selection, the appropriate digitised signal was readout from the ADCs. From the beginning of the ADC gate to the end of the ADC readout, the discriminator inputs were vetoed.

The electronics specific to the control of the BDD-motion and of the X-ray tube operation are shown at the bottom of Fig.4.

Rotations of the BDD around the g_{φ}-axis and the g_{ϑ}-axis are implemented by two stepping motors driven by a stepping motor driver unit. The angles of rotation are measured by two precise angle encoders from HEIDENHAIN.

The rotations around the g_{ϑ}-axis are encoded by an absolute angle encoder (ROC417), which uses photo-electric scanning. The measuring standard for this encoder is a glass disk with coded gradations. It resolves one revolution out of 131072 positions, each of which corresponds to a definite value of a purely binary 17-bit output synchronous-serial code following RS-422 standards. An

quanta in the wire-material (CuBe or tungsten) and in the gas mixture in the straws. Indeed, this absorption cross-section for 36 keV X-rays is 4.5 times larger in the Cu-Be wires than in the Ar-CO_2 gas mixture. Since the absorption of X-rays in this energy range is mainly through atomic photo-effects on the K-shell, photoelectrons of 27.05 keV and 32.08 keV are produced in the copper and argon respectively. Subsequent radiation through Auger electrons or fluorescent X-ray emission, in order to fill the vacancy in the K-shell, also contributes to the measured signal. The mean free path of photoelectrons in the Cu-Be wire itself is $\sim$ 1.5 μm, and therefore only photoelectrons produced in a thin layer of the wire periphery can produce a signal in the straw. On the other hand, the mean free path of X-rays of $\sim$ 8 keV produced through fluorescent K_α-radiation in the copper, is about 22 μm inside the wire itself. As a consequence, even for a wire diameter of 50 μm, an X-ray signal may be observed in the straws for X-rays absorbed over the full thickness of the wire.

The measurement procedure of the wire coordinates in the wheel is the same as was used in the calibration procedure with the metrology wheel. Therefore, the reader is referred to [1] for a more complete discussion of this procedure and of the parameters defining the equations of the wire projections.

The BDD operated automatically under the control of a PC. For a fixed elevation angle ϑ, it was possible to irradiate with the X-ray beam all straws and wires by rotating the BDD step by step around the g_φ-axis. During one scan, which was limited in scope by the amount of readout electronics, as many as 64 wire profiles could be measured. These measurements were then repeated for another value of the elevation angle ϑ. As depicted in Fig.3, each wire can be represented by a straight segment defined by its extremities at the innermost and outermost radii, which correspond to the elevation angles ϑ_{inner} and ϑ_{outer}.

The elevation angles ϑ_{inner} and ϑ_{outer} were chosen to be 25.2^o and 37.7^o respectively, for all straw layers measured by this procedure. These values of ϑ_{inner} (respectively ϑ_{outer}) corresponded to the smallest (respectively largest) possible elevation angle for the first (respectively last) layer of the straws seen by the X-ray beam, such that the wide component (along the wire) of the X-ray beam was always fully contained within the straw tube.

The exposure time per point, which depends upon the X-ray beam counting rate as a function of the depth of the straw layer being measured, was chosen typically to be between 3 and 10 seconds, such that the centre of gravity of the wire profile was measured to an accuracy of better than 10 μm. The measurement step was approximately equal to the wire diameter of 50 μm, i.e. $20''$ in case of

To establish the position of the geometrical centre of the wheel, measurements of high-precision markers placed on the wheel [3] carried out by the survey group were used. For this purpose, a tungsten wire cross of 200 μm diameter was placed on the wheel through the centres of these markers. The BDD was placed on a rigid table at a distance of 1130$\pm$5 mm measured from the crossing point of the rotation axes to the front-plane of the wheel.

To find the position of the X-ray beam in space, two tungsten wires of 50 μm diameter, serving as threads for a lead weight were placed into the X-ray beam, one of them close to the exit slit and the other close to the front-plane of the wheel. An additional wire was placed behind the wheel close to its back-plane. The position of this third wire was used to determine the angle between the g_φ-axis and the plane of the wheel. The beam profile was measured by observing the wire shadows on a NaI detector placed behind the wires. Using the position of these wires and a theodolite, placed behind the wheel at a distance of $\sim$1 m, the position of the X-ray beam with respect to the centre of the wheel was adjusted with the required accuracy.

An even finer adjustment may be carried out by comparing the width of the measured wire profiles over various parts of the wheel (e.g. wires disposed at the top, bottom, right and left of the wheel). The width of the measured wire profile is determined by the convolution of the X-ray beam profile and the expected wire profile. To a good approximation, it can be assumed that these profiles have a rectangular shape with a width of 100 μm for the X-ray beam profile and of 50 μm for the expected wire profile. Therefore their convolution should have a trapezoidal form with a width (FWHM) of $\sim$ 100 μm. If the width of the wire profiles measured over various parts of the wheel are different one from the other and from the theoretical values, the BDD must be adjusted to minimise this difference. This finer adjustment was not used for the measurements reported here, due to the long set-up time needed to prepare one cell for measurements (about 1-2 days).

Fig.2 shows schematically the BDD placed on a rigid table in front of the endcap TRT wheel prototype for the measurements of the wire positions.

4 Measurement procedure

The measurement of the wire positions inside the straw drift-tubes exploits the large difference between the photo-electric absorption cross section of X-ray

128 straws each. The angle between the centres of neighbouring straw location holes in each layer is equal to 2160″, i.e. the distance between these hole centres is equal to 5248.8 μm at the radius of the inner wheel and 10497.6 μm at the radius of the outer wheel. The angular offset between the first nine layers is set to 3/8 of 2160″ (810 ″) in the anti-clockwise direction. The angular offset between the next seven layers is set to the same value, but in the clockwise direction. Therefore, only two wire projections overlap one another exactly in the direction perpendicular to the wheel layers.

The X-ray measurements were performed with the straws filled with an 90%Ar+10%CO_2 gas mixture at atmospheric pressure.

3 Adjustment of the BDD relative to the wheel

A precise adjustment of the X-ray beam relative to the wheel was performed in order to :

- set the X-ray beam direction perpendicular to the plane of the wheel;
- dispose the BDD, so that its azimuthal rotation axis g_φ crosses the wheel plane in its centre of symmetry.

The centre of symmetry of the wheel is determined as the average value of the crossing points between all wire pairs. But, before the measurements are performed, the position of this centre of symmetry is unknown. Therefore, the basic initial assumption is that it coincides with the geometrical centre of the wheel.

The exit slit of the BDD has a width of $\sim$ 50 μm and a height of $\sim$ 22 mm. The first adjustment step was to align the wide component of this exit slit along the vertical axis, that is parallel to the straw wires. After adjustment, the direction of the X-ray beam coincided with the g_φ-axis with an accuracy of better than 10 μm in the horizontal direction (narrow component of exit slit) and better than 100 μm in the vertical direction (wide component of the exit slit). The angle between the g_φ-axis and the X-ray beam was estimated to be less than 3.5″.

The adjustment of the X-ray beam relatively to the centre of symmetry of the wheel has to be better than 50 μm in the horizontal direction and 500 μm in the vertical direction. The projection of the BDD exit slit onto the wheel plane will then be parallel to the wire projection for any value of the φ-rotation angle.

1 Introduction

In an earlier report [1], a detailed description of the Beam Directing Device has been given. The BDD provides the possibility to direct a narrow monochromatic X-ray beam in a chosen direction within some solid angle and to measure the angular position of this beam with an accuracy of $0.2''$ for the azimuthal angle and of $10''$ for the elevation angle. When the X-ray beam irradiates the wire inside a straw drift-tube, a sharp increase of the counting rate in this tube is seen [2]. By keeping track of the angular position of the X-ray beam, the wire position can be accurately determined.

This report contains the results of the wire-position measurements performed by the BDD on the full-scale endcap TRT prototype. This engineering prototype was constructed to get experience with straw assembly and gas circulation, but mainly with the mechanical precision and stability of the assembled wheel.

2 Description of the full-scale TRT prototype

Fig.1 shows a photograph of the full-scale endcap TRT wheel prototype. This is a complete azimuthal wheel containing 9 600 cylindrical straw drift-tubes [3] distributed in 16 planes or layers. These layers are interleaved with polypropylene foil radiators to produce transition radiation. The straws have a length of ~ 500 mm and a diameter of 4 mm and are reinforced with carbon-fibres to avoid the influence of humidity and temperature on the properties of the detector. They are prepared from a kapton film coated with a conductive layer (2000 $\mathring{A}$ Al + 6 μm carbon-loaded kapton). The total wall thickness of a straw tube is about 60 μm. The straws are fixed into and supported by an inner and an outer wheel. The location holes for the straws were drilled with an accuracy of better than 20 μm. The straws were equipped with copper-beryllium wires of 50 μm diameter[2].

The expected mechanical accuracy of the wire installation with respect to the hole centre was $\sigma_{expected} \sim 30$ μm for the inner wheel, and $\sigma_{expected} \sim 40$ μm for the outer wheel. An additional contribution to this accuracy of up to 200 μm wheel is expected for the outer from the fixation of the non-cylindrical straws equipped with carbon-fibres into the cylindrical holes (the carbon-fibre reinforcement was implemented after the outer wheel design). The wheel is divided into 75 cells of

[2] About 10% of the straws were equipped with 30μm diameter wires

Contents

ATLAS Internal Note
INDET-NO-162
1 March 1997

An X-Ray Measurement Station for the ATLAS Endcap TRT Calibration.

Part 2: Results from the measurements of the full-scale endcap TRT wheel prototype.

V. Ivanov, O. Fedin, A. Jelamkov, S. Muraviev[1],
Yu. Platonov, A. Smirnov

PNPI, St.-Petersburg

Abstract

This note presents the results of the wire-position measurements performed by a Beam Directing Device (BDD) on the full-scale endcap Transition Radiation Tracker (TRT) prototype. The aim of the measurements was to check the mechanical tolerance of the wire installation in view of the decisions to be taken for the final design of the endcap TRT. The results of the measurements show that the wires are positioned to an accuracy of 20 μm to 80 μm well within the specifications requiring an overall tolerance of ± 100 μm.

[1]Lebedev Physical Institute, Moscow